Fracture Tests of Etched Components Using a Focused Ion Beam Machine

Jonathan L. Kuhn[a], Rainer K. Fettig[b], S. Harvey Moseley[a], Alexander S. Kutyrev[b], Jon Orloff[c]

[a]NASA/Goddard Space Flight Center, Greenbelt, MD
[b]Raytheon ITSS, Greenbelt, MD
[c]Department of Electrical Engineering, University of Maryland College Park, MD

ABSTRACT

Many optical MEMS device designs involve large arrays of thin (0.5 to 1 μm) components subjected to high stresses due to cyclic loading. These devices are fabricated from a variety of materials, and the properties strongly depend on size and processing. Our objective is to develop standard and convenient test methods that can be used to measure the properties of large numbers of witness samples, for every device we build. In this work we explore a variety of fracture test configurations for 0.5 μm thick silicon nitride membranes machined using the Reactive Ion Etching (RIE) process. Testing was completed using an FEI 620 dual focused ion beam milling machine. Static loads were applied using a probe, and dynamic loads were applied through a piezo-electric stack mounted at the base of the probe. Results from the tests are presented and compared, and application for predicting fracture probability of large arrays of devices are considered.

Keywords: stiffness, strength, fracture, fatigue, silicon nitride, micro-shutters, torsion, hinge

1. INTRODUCTION

Brittle materials such as silicon and silicon nitride are being used as structural materials in micro-electromechanical systems (MEMS) in ways that are not possible in large scale structures. In particular, overall small component size and low flaw density result in significantly higher strength than the bulk material. Modern fabrication techniques also enable construction of high aspect ratio MEMS components. These two factors may be combined to generate unusual structural designs that involve extremely large deformations of brittle materials.

In previous work we used a focused ion beam (FIB) machine to explore applying the above principles to develop a torsional flexure hinged micro-shutter that survives over 90 degrees of twist. Results from those studies are presented

Send correspondence to R.K.F. E-mail: Rainer.Fettig@gsfc.nasa.gov

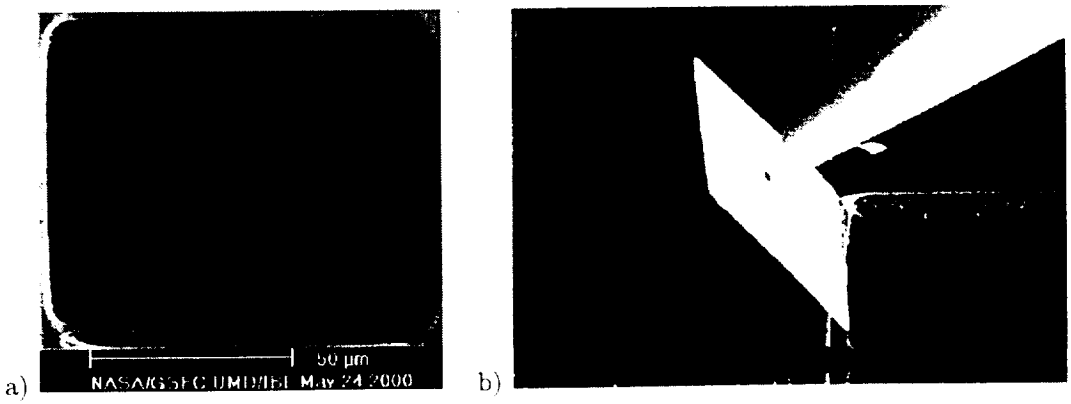

Figure 1. a) Single etched silicon nitride micro-shutter. b) Micro-shutter rotated approximately 135 degrees.

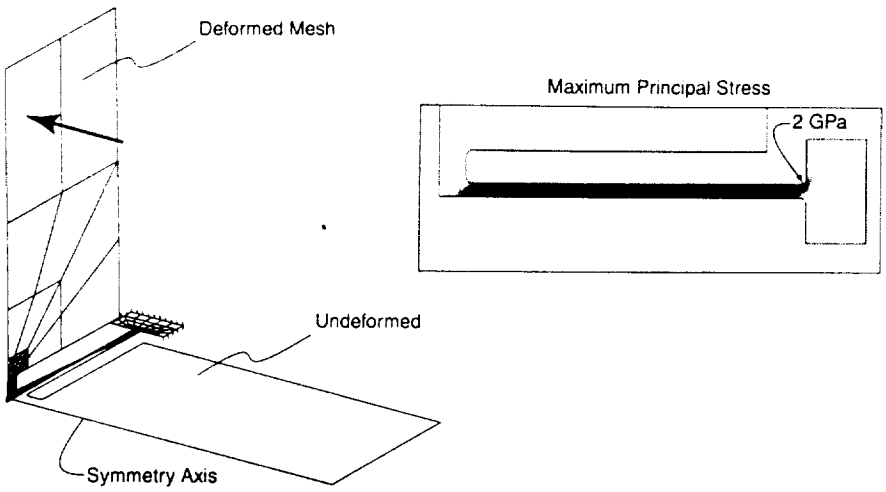

Figure 2. Silicon nitride micro-shutter finite element model.

in Refs. 1 and 2. In the above work, individual micro-shutters and bending test structures were milled and tested using the FIB machine. Tests were completed using components fabricated from both 2.0 μm thick single crystal silicon and 0.5 μm low stress silicon nitride suspended membranes. Based on these studies, we selected 0.5 μm silicon nitride to fabricate large arrays of micro-shutters[3,4] using reactive ion etching (RIE) as shown in Fig. 1.

In the above figure, the etched shutter array is shown on the left, and one of the shutters is shown rotated approximately 135 degrees out of the array plane on the right. During operation these shutters will be subjected to a large number of rotations to 90 degrees at temperatures of 30 K over a 10 year flight life.[3] Detailed finite element analysis as shown in Fig. 2 predicts peak maximum principal stresses in the silicon nitride torsion bar on the order of 2 GPa at room temperature. This stress is a result of the local rounded corner stress concentration and combined torsion and lateral loads in the 90 degree position. These relatively complicated high stresses introduce significant risk of failure for the brittle structures. As a result rigorous engineering test and analysis is required to ensure a low failure rate over the life of operation.

Our objective is to develop test methods that closely match the size, shape, fabrication process, and loading environment of the micro-shutter application. A large number of fracture tests will yield the data necessary to complete Weibull statistical analysis as described in Ref. 5, allowing for a prediction of the probability of fracture under static loading. While silicon nitride is known to be a brittle material not susceptible to fatigue failure, the effects of an extremely low population of flaws combined with extremely high stresses are not well known. As a result, torsional high cycle tests are required to validate that the shutter strength will not degrade over time due to operational cycles.

In this work, the methods developed in Refs. 1 and 2 are expanded to include a torsional test and the series of tests are applied to silicon nitride components fabricated using reactive ion etching instead of the FIB machine. In particular, we use a resonating cantilever beam, bending fracture, and torsion fatigue test to help determine how reliable the torsional flexure hinges will be during operation. In this paper we present a brief overview of the tests followed by results for etched silicon nitride structures.

2. EXPERIMENTAL METHODS AND THEORY

Our goal is to develop relatively simple tests that allow us to predict the performance and reliability of the flexure hinges for a large number of load cycles operating at 30 K. Ideally these tests should simulate the operating environment as closely as possible, while still allowing for simple theoretical predictions to enable design optimization.

Currently, we use a resonating cantilever beam test to experimentally measure the Young's modulus of the silicon nitride membranes. While the membrane modulus should not differ significantly from bulk properties,[6] this test helps to validate our experimental procedures. We also use a dual width bending test specimen presented in Ref. 2

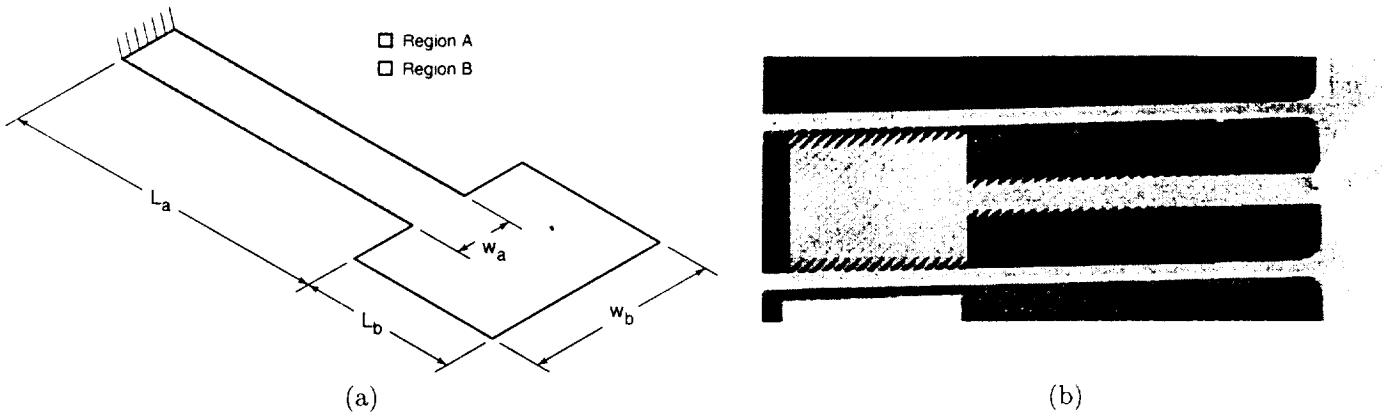

Figure 3. a) Vibration test schematic drawing. b) *In situ* vibration test specimen under an applied periodic load applied at the fixed end.

to measure the static strength of the silicon nitride membrane. This bending test is relatively insensitive to the input load position, and failure occurs due to stress concentration, which is similar to our device primary mode of failure. However, the bending test failure occurs due to a peak longitudinal stress while the primary contribution of stress in the micro-shutter is due to torsion. The micro-shutter itself may also be a good torsional test specimen, however, a lateral component of force is applied during operation to induce torsion, which bends the torsion beams and complicates the theoretical analysis. We have experimented with a symmetric torsional test. The goal of the torsional test is to rapidly apply a large number of load cycles to assess the sensitivity to torsional fatigue failure.

In this section we present a description of the tests along with the theoretical equations derived and compared with finite element analysis results presented elsewhere.[1,2]

2.1. Materials, Fabrication, and Testing

Tests and observations were completed using an FEI 620 focused ion beam milling machine. The FEI 620 is a dual beam machine, with an ion and electron column, which allows ion milling and *in situ* scanning electron microscopy. Ion milling can be performed with ion beam spot sizes of 20 nm to 1 μm and machining rates in silicon up to 10 $\mu m^3/s$. The machine is also equipped with a micro-manipulator needle and the ability to deposit platinum by ion induced metal organic chemical vapor deposition (MOCVD).

All components and test specimens presented in this paper were bulk micro-machined in a two stage process, starting from a 100 μm thick silicon wafer coated with 0.5 μm of silicon nitride. In the first stage, the silicon is back etched with DRIE, leaving a suspended silicon nitride membrane. In the second stage the membrane is etched with RIE to yield the micro-structural elements such as micro-shutters or test specimens. A more detailed description of the fabrication process is included in a companion paper.[4]

A variety of test specimen shapes and sizes were included in the mask design. Only a few were used for actual testing. These included micro-shutters with torsion bar width greater than 2 μm, resonating beams, dual width bending test structures with neck width and length greater than 3 μm and 6 μm, respectively, and torsional test structures. An overview of these test structure designs and theory are presented in the following sections.

2.2. Resonant Stiffness

In general it is difficult to measure the Young's modulus of micro sized structures. In static load tests, such as tension and bending tests, both the strain and load must be measured accurately. The most reliable methods are based on tension tests, in which the load is measured directly, and strain is measured using laser interferometry.[7] As a first order approximation, we assume that the elastic properties of our micro samples are approximately equal to those of the bulk materials with similar micro-structure, and measure the Young's modulus using a resonating beam to validate our test measurements and procedures. If there is strong confidence in the Young's modulus from other sources, then this test may be used to determine the membrane thickness.

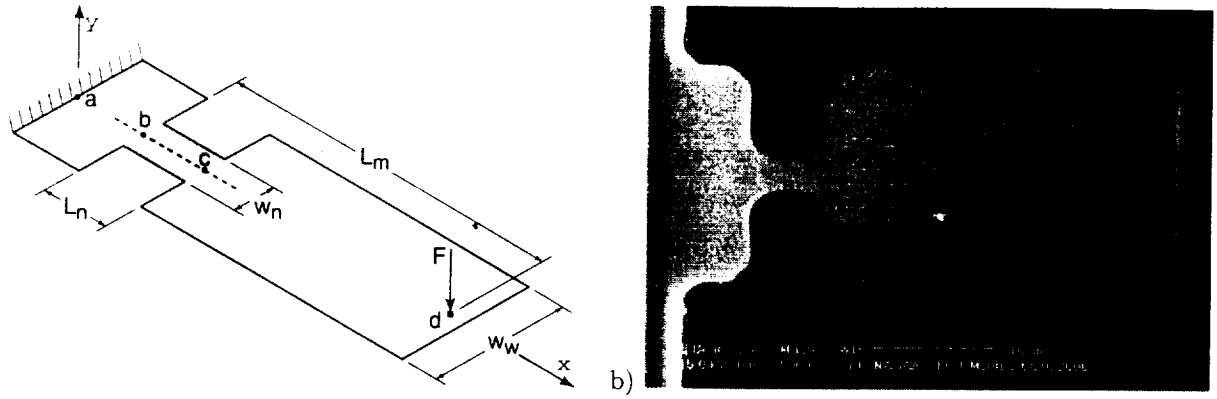

Figure 4. a) Bending test schematic drawing. b) Scanning electron micrograph of an etched silicon nitride bending test specimen.

In this test, a long slender cantilever beam is fabricated with a wide end region as shown in Fig. 3 to produce a mass/spring system, whose first natural frequency can be measured and computed analytically. In the experimental setup, the beam is pushed vertically with a needle and released. The approximate natural frequency is measured by pointing the electron beam in a fixed position where the vibrating cantilever beam moves in and out of the electron beam path. This modulates the secondary electron detector signal with the frequency of the vibration. This signal is acquired with an oscilloscope and the period of the vibration is determined. Subsequently, a needle mounted on a piezo-electric crystal is pushed against the fixed end of the cantilever beam and a periodic movement is applied. The frequency of the needle vibration is varied over a small range around the approximate value previously determined. The response is monitored as above, and the frequency of peak displacement is recorded.

Once the fundamental natural frequency is measured, the Young's modulus may be computed from:

$$E = \frac{16\pi^2 f^2 L^4 \rho}{t^2}\left(\frac{w_b}{w_a}\frac{L_b}{L} + C_1\frac{L_a}{L}\right). \tag{1}$$

where the constant C_1 equals 0.2357,[8,9] f is the cyclic natural frequency in Hz, and L_a, L_b, w_a, and w_b are the lengths and widths, respectively, of the beam regions as shown in Fig. 3. The parameter $L = L_a + L_b/2$ is the cantilever length to the center of the end mass, ρ is the mass density, and t is the thickness. The formulation of equation (1) and comparison with detailed finite element analysis results are presented in Ref. 1. Note that the above equation may be used to solve for the membrane thickness if the Young's modulus is given.

2.3. Bending Strength

In order to determine the material static strength, we use a dual width bending test specimen as shown in Fig. 4. The structure is a cantilever beam with peak stress occurring in the narrow region at the end farthest from the applied vertical load. The wide portion of the beam is designed to be stiff relative to the narrow region. This configuration drives most deformation into the narrow region, resulting in smaller failure angles. This test specimen is also relatively insensitive to the loading position.

For this test we gradually apply a vertical load at the end until the specimen fails, and record the image sequence leading to failure. The image just prior to failure is analyzed to extract the relative angle at failure. This measurement is used in conjunction with a presumed Young's modulus of the bulk material, or the Young's modulus measured using the resonant test, and the following equation to compute the stress at failure.

$$\sigma_{xx}^{eq} = \frac{Et(\theta_c - \theta_b)}{2L_n\left(1 - \frac{1}{2\alpha}\right)} \tag{2}$$

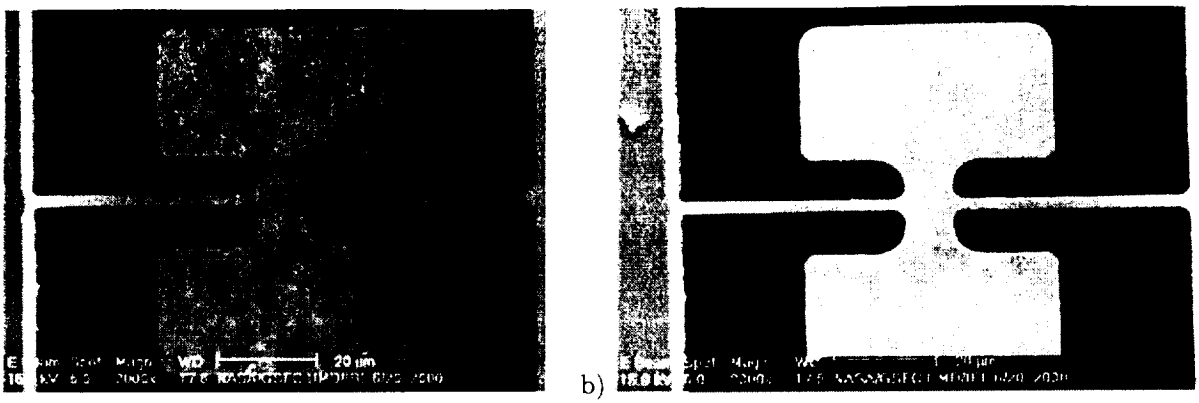

Figure 5. a) Initial symmetric torsional test specimen. b) Torsional test specimen cut in the FIB machine to produce asymmetry.

where σ_{xx}^{eq} is the theoretical peak stress, $\theta_c - \theta_b$ is the relative rotation across the narrow region, and L_n is the length of the neck region as shown in Fig. 4a. The parameter $\alpha = L_m/L_n$, where L_m is the approximate moment arm of the applied load relative to the anticipated failure location. As mentioned above equation (2) is relatively insensitive to small changes in α. The formulation of equation (2) and comparison with detailed finite element analysis results for 2.0 μm thick single crystal silicon are presented in Ref. 2.

In previous work, we found it difficult to accurately measure the inclination angles at points b and c. In the case of etched silicon nitride membranes presented in this paper, the specimens that survived etching did not have a uniform width in the neck region, which made these measurements even more difficult. As a result, we use detailed finite element analysis to compute the peak maximum principal stress. In this approach we measure the inclination of the wide portion of the beam and correlate with the finite element stresses instead of measuring the angles at points b and c and using equation (2). This procedure is significantly easier experimentally and more accurate, while the benefits of load position insensitivity and relatively low fracture angles are retained.

2.4. Torsional Fatigue

The ultimate survival test for the torsional flexure hinged micro-shutters is to fabricate the shutters, and fold each one beyond the 90 degree requirement, preferably all the way to 180 degrees, and preferably at cryogenic temperatures. However, due to the combined load state and local stress concentrations, the stresses may only be calculated using detailed finite element results. During the development stages it is difficult to apply a large number of load cycles to these shutters. Also these shutters, by design, are not intended to fail. It is important to test to failure to establish precisely the realized factor of safety.

As a result we seek a torsional test that allows us to apply a large number of cycles in a short period of time. This test should sustain significantly high stresses that can be varied with specimen dimensions. Ideally the stresses should be predictable with relatively simple theoretical equations.

In this attempt to develop such a torsion test specimen, we fabricated a variety of symmetric torsion structures. One such specimen is shown in Fig. 5. The intent is to resonate the torsion bar for extended periods of time to determine if there are fatigue effects. We may also ramp the energy input until failure, while monitoring the rotation angle.

In the above configuration, for a given torque T the maximum shear stress (neglecting stress concentrations) is[8,9]

$$\tau_{max} = \frac{3T}{8ab^2}\left[1 + 0.6095\frac{b}{a} + 0.8865\left(\frac{b}{a}\right)^2 - 1.8023\left(\frac{b}{a}\right)^3 + 0.9100\left(\frac{b}{a}\right)^4\right] \qquad \text{for } a \geq b \tag{3}$$

where a is half the long edge of the rectangular section, and b is half the short edge. The torque T is related to the twist angle θ by

Table 1. Young's modulus computed from equation (1) and frequency measurements for various thicknesses.

Thickness (μm)	Average Young's Modulus (GPa)
0.40	359
0.45	284
0.50	230
0.55	190
0.60	160

$$T = \frac{\theta K G}{L} \tag{4}$$

where

$$K = ab^3 \left[\frac{16}{3} - 3.36 \frac{b}{a} \left(1 - \frac{b^4}{12a^4} \right) \right],$$

L is the torsion bar length, and G is the modulus of rigidity. We have found from detailed finite element analysis that while the geometry changes are highly nonlinear, the stress remains proportional to the twist angle. Details of the finite element validation are presented in Ref. 1.

The above equations neglect the concentration in stress at the end of the torsion bars, and the equations are approximate. As a result we use this test to qualitatively determine if the material is susceptible to fatigue crack growth, and to what extent. While fatigue fracture of a brittle material in a vacuum is unlikely at normal scales at room temperature or below, the extreme levels of stress compel us to confirm what the life expectancy will be in flight.

A key challenge in the torsional test is how to induce large rotations without adding significant lateral bending moments. We have attempted placing an electrode near the end of a blade in both shutters and the symmetric torsion specimen. A periodic voltage is applied at the resonating frequency of the structure. However, the force is proportional to the square of the distance, and as a result, this approach never achieves large rotation angles.

An alternative is to use a stiff probe mounted to the end of a piezo-electric stack to mechanically drive the deformation. In this approach, the end of the probe is pushed lightly against the torsion bar near a fixed end. A periodic displacement with small magnitude is applied normal to the plane of the specimen at the resonating frequency of the specimen. The intent is to drive energy into the specimen at resonance, resulting in large displacements. However, we found that this configuration does not work for the symmetric torsion specimen. Therefor, we cut away a portion of one blade to create asymmetry as shown in Fig. 5b.

3. RESULTS OBTAINED WITH ETCHED SILICON NITRIDE

Experiments were completed using each of the test structures etched from silicon nitride as described above. For the resonant stiffness test, cantilever beams with lengths of $L_a = 252$, 243, and 237 μm were fabricated. The remaining parameters were the same for each specimen. These dimensions consisted of widths $w_a = 40$ μm and $w_b = 160$ μm, and length $L_b = 120$ μm. We assumed the density of silicon nitride to be $\rho = 3.0 \times 10^{15}$ $Kg/\mu m^3$. Frequencies for the three different length specimens were measured to be $f = 2740$, 2830, and 2940 Hz, respectively. While the nominal thickness of the silicon nitride membrane is approximately $t = 0.5$ μm, it is difficult to accurately measure this dimension. As a result the average Young's modulus for several thicknesses were computed using equation (1) and listed in Table 1.

The Young's modulus of bulk silicon nitride is known to be in the range of 207 to 310 GPa.[10] Tabata *et. al.*[11] reported a Young's modulus of 290 GPa for 0.5 μm thick low pressure chemical vapor deposited (LPCVD) silicon nitride film, which matches the material considered herein. Solving equation (1) for the thickness, assuming a modulus of 290 GPa, yields $t = 0.445$ μm. It is very likely that the actual thickness of our membranes are closer to 0.445 μm than to the nominal thickness of 0.5 μm.

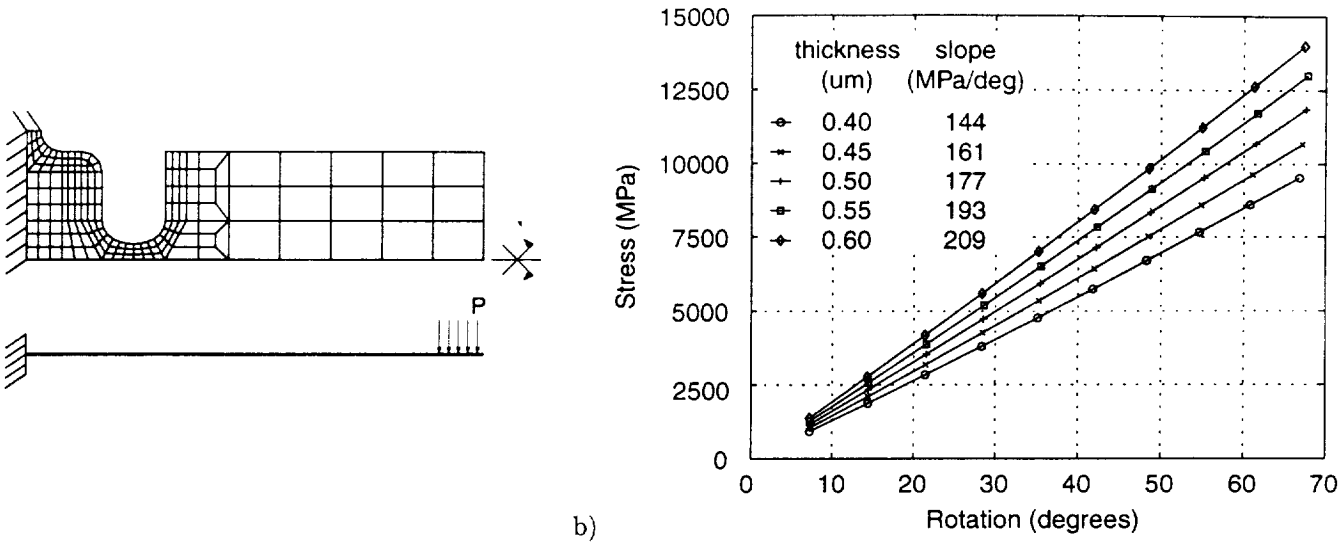

Figure 6. Non-linear finite element analysis. a) Mesh of one symmetric half of the bending specimen. b) Maximum principal stress versus angle for various thicknesses.

Bending test structures were also tested by the procedure outlined in the previous section. A total of 47 specimens with nominal dimensions of $L_n = 6\ \mu m$, $w_n = 3\ \mu m$, $L_m = 36\ \mu m$, $w_w = 20\ \mu m$, and nominal thickness $t = 0.5\ \mu m$ were loaded to failure. A finite element model of this geometry was created as shown in Fig. 6a. Based on the above resonant beam tests, a Young's modulus of 290 GPa was assumed for the silicon nitride membrane. The model was fully constrained at the base were the membrane meets with the full 100 μm thick silicon wafer. A follower pressure load was applied to induce the rotation, and the geometric non-linear solution sequence in UAI/NASTRAN was used to solve the boundary value problem.

The stresses were monitored as a function of blade rotation at each load step, and the results are plotted in Fig. 6b. The above procedure was repeated for various thicknesses in the range of $t = 0.40$ to $0.60\ \mu m$. Fig. 6b shows that even though the displacements are large and non-linear, the stress remains a linear function of rotation angle, and the slope of these curves are included in the plot.

Each of the 47 bending test specimens were loaded to failure, and the angle just prior to failure was measured using the techniques outlined in the previous section. A fracture surface from one test specimen is shown in Fig. 7a. The small size of these specimens are difficult to resolve using scanning electron microscopy. However, the image shows the location of the fracture, and also the inclined sides and sharp edges of the specimen due to the etching process. Based on the resonant beam test results described above, the thickness of the test specimens were assumed to be $t = 0.45\ \mu m$. Consequently, the slope of 161 MPa/deg shown in Fig. 6b for $t = 0.45\ \mu m$ was used to compute the stress at fracture for each test. The average fracture stress was found to be $\sigma_f = 7.0\ GPa$ with a standard deviation of 0.9 GPa. The lowest stress was 5 GPa giving an approximate factor of safety of 2.5 GPa for the micro-shutter design presented in Fig. 2. This factor of safety is relatively low given the brittle material subjected to a high stress. These results gave a distribution which can be used to compute the Weibull distribution parameters, and compute more accurately the probability of failure. Unfortunately, the statistical analysis was not completed at the time of submission of this paper.

Some asymmetrical torsional specimens were tested as described in the previous section, and shown in Fig. 7b. All samples eventually failed due to effects of the tip, such as handling, pressure to the beam, or impact during vibration coupling. In the last case material was physically moved or distorted at the tip location. The setup up was unstable and not reproducible. However, it was possible to achieve significant vibrational amplitudes. A torsional specimen with a $2.9 \times 46\ \mu m$ beam was driven at about 62 kHz for longer than 1 minute to intermittent amplitudes ranging roughly between 20 to 90 degrees. A second specimen with a $3.9 \times 35\ \mu m$ beam at 88 kHz survived for longer than 5 minutes at 20 to 60 degrees. We observed no change in resonant frequency and no obvious fatigue

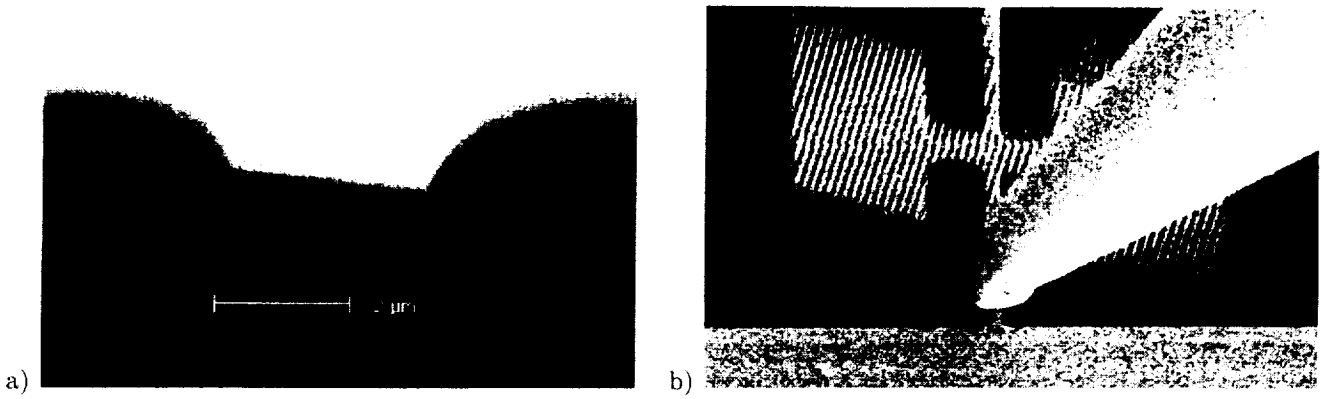

Figure 7. Fracture test results. a) Static bending test fracture surface. b) Torsional fatigue test.

failure.

In future work, we will attempt larger displacements and a more reproducible setup by modifying the sample geometry, for example, by adding small offset tabs near the base of the torsion beam to facilitate asymmetric mechanical driving input.

4. CONCLUSION

The objective of this work is to determine the reliability of a torsional flexure hinged micro-shutter for cryogenic space flight applications. To this end, we have developed a series of tests to validate our procedures, measure the static strength, and qualitatively predict the likely-hood of fatigue fracture. In previous work, these tests were used to study structures fabricated using a FIB milling machine. In this work, we further developed the tests and applied them to etched silicon nitride structures.

The resonant stiffness test yielded results consistent with those presented in the literature. The bending fracture tests were found to be convenient and provided sufficient data to pursue statistical analysis. The preliminary torsional tests showed that at low stress levels there is no evidence of fatigue in the silicon nitride membranes studied.

All of the tests to date have been completed at room temperature. In future work, these tests must be repeated at cryogenic temperatures to validate the torsional flexure hinged design for long term cryogenic space flight applications.

ACKNOWLEDGMENTS

This project was supported by a grant from NGST GSFC 98-01 and NASA 98-10. The authors gratefully acknowledge Brent Mott from NASA/GSFC Code 553 and Mary Li from Raytheon ITSS for the fabrication of the test structures, and Tim Carnahan from NASA/GSFC Code 542 for assistance with image processing.

REFERENCES

1. R. Fettig, J. Kuhn, S. Moseley, A. Kutyrev, J. Orloff, and S. Lu, "Some aspects on the mechanical analysis of micro-shutters," in *Micromachining and Microfabrication, Proceedings of SPIE* **3875**, Sept. 1999.
2. R. Fettig, J. Kuhn, S. Moseley, A. Kutyrev, and J. Orloff, "Fracture probability of mems optical devices for space flight applications," in *Microscale Systems: Mechanics and Measurements Symposium, Proceedings of SEM* , June 2000.
3. S. Moseley, R. Fettig, A. Kutyrev, C. Bowers, R. Kimble, J. Orloff, and B. Woodgate, "Programmable 2-dimensional microshutter arrays," in *Micromachining and Microfabrication, Proceedings of SPIE* **3878**, Sept. 1999.
4. S. Moseley, R. Fettig, A. Kutyrev, M. Li, D. Mott, and B. Woodgate, "Status of the development of a 128x128 micro-shutter array," in *Micromachining and Microfabrication, Proceedings of SPIE* **4178**, Sept. 2000.

5. S. Greek, F. Ericson, S. Johansson, and J. Schweitz, "In situ tensile strength measurement and weibull analysis of thick film and thin film micromachined polysilicon structures," *Thin Solid Films* **292**, pp. 247–254, 1997.
6. J.-A. Schweitz and F. Ericson, "Evaluation of mechanical materials properties by means of surface micromachined structures," *Sensors and Actuators* **74**, pp. 126–133, 1999.
7. W. Sharpe, B. Yuan, R. Vaidyanathan, and R. Edwards, "Measurements of young's modulus, poisson's ratio, and tensile strength of polysilicon," in *MEMS97, Proc. 10th IEEE Workshop* , pp. 424–429, 1997.
8. W. D. Pilkey, *Formulas for stress, strain, and structural matrices*, J. Wiley, New York, 1994.
9. W. C. Young, *Roark's Formulas for Stress and Strain*, McGraw-Hill, Inc., New York, 1989.
10. D. R. Askeland, *The Science and Engineering of Materials, Second Edition*, PWS-KENT, Boston, 1989.
11. O. Tabata, K. Kawahata, S. Sugiyama, and I. Igarashi, "Mechanical property measurements of thin-films using load deflection of composite rectangular membranes," *Sensors and Actuators* **20**, pp. 135–141, Nov. 1989.